Journal of Applied Fluid Mechanics, Vol. 9, No. 6, pp. 3087-3100, 2016.
Available online at www.jafmonline.net, ISSN 1735-3572, EISSN 1735-3645.

Vortex Interaction and Roll-Up in Unsteady Flow past Tandem Airfoils

H. Aziz[1] and R. Mukherjee[2†]

[1] *Department of Mechanical and Nuclear Engineering, Virginia Commonwealth University, Richmond, Virginia, USA 23284*
[2] *Department of Applied Mechanics, Indian Institute of Technology Madras, Chennai, India 600036*

[†]*Corresponding Author Email: rinku@iitm.ac.in*

(Received December 30, 2014; accepted February 21, 2016)

ABSTRACT

A discrete vortex model coupled with a vortex dissipation and vortex core criteria is used to study the unsteady flow past two airfoils in configuration. The unsteady wakes of the airfoils are modeled by discrete vortices and time-stepping is used to predict the individual wake shapes. The coupled flow is solved using a combined zero-normal flow boundary condition and Kelvin condition which result in $(2N+2)X(2N+2)$ equations. Results are presented showing the effect of airfoil-airfoil and airfoil-wake interaction on the aerodynamic characteristics of the configuration. The effect of relative velocity, rate of pitching and phase-lag are studied on airfoil performance and wake shape is predicted.

Keywords: Airfoil; Vortex interaction; Unsteady; Aero-dynamics; Numerical singularity.

NOMENCLATURE

C_l	coefficient of lift	t	latest time step
C_m	coefficient of pitching moment	V	airfoil velocity
C_d	coefficient of induced drag	Φ	velocity potential
c	airfoil chord length	Ψ	stream function
h_o	amplitude of heaving motion	Γ_f	circulation of the airfoil
$\hat{n}$	unit vector normal to a solid surface	Γ_W	circulation of the wake
O, o	origin of fixed and moving reference frames	σ	radius of the vortex core
U_∞	free-stream velocity	ω	angular frequency of heaving motion
r	distance between free vortex and solid surface	α	angle of attack

1. INTRODUCTION

Studies of unsteady aerodynamics of pitching airfoils are in crucial need in wind turbines, more specifically in rotorcraft dynamics. More recently, studies on unsteady aerodynamics of airfoils have been motivated by the prospect of utilizing the advantages of large un-steady aerodynamic forces for aerospace applications like increased maneuverability of fighter aircraft, use of micro-UAVs, which are designed for very small payloads for remote-sensing operations in areas of limited access and the use of multi-UAVs in formation for surveillance purposes to increase their longevity and endurance. In addition to the knowledge required for unsteady flow-field aerodynamics of single airfoils, in most of the applications mentioned above, the airfoils also operate in close proximity to each other so that their flow-fields overlap. Hence, an accurate estimate of the flow-field and the knowledge of flow patterns and structures are inevitable for the successful design and modeling of these applications.

The unsteady aerodynamics of airfoils has been studied by researchers both as a practical problem as well as an important fundamental one. Wu, Wang and Tuncer (1986) studied the dynamic stall of an airfoil pitched rapidly at a constant rate to large angles of attack computationally. Greenwell (2004) reviewed approaches to modeling the unsteady

aspects of the aero-dynamic characteristics of maneuverable aircraft. Hall and Clark (1993) presented a linearized Euler solver to calculate the unsteady flows in turbomachinery blade rows due to both incident gusts and vibrations of the blade. Capece and Fleeter (1986) studied the effects of steady loading and the detailed aerodynamic forcing on airfoil row unsteady aerodynamics at low reduced frequency values.

The unsteady aerodynamics of pitching airfoils involves an additional unsteady lift, which is due to the vortex that forms near the leading edge during the pitching motion and convects downstream. Fulayter, Lawless and Fleeter (2002) studied the phenomenon of dynamic stall itself besides the aerodynamics of unsteady flight. Jose and Baeder (2009) studied the 2D unsteady aerodynamics of trailing edge flap-tab airfoils with overhang and gap both analytically and using CFD. Bacic (2008) experimentally predicted and tested the ac-curacy of the free flight unsteady aerodynamics of a pitching airfoil at high angles of attack.

Fritz and Long (2004) used an unsteady vortex lattice method to study oscillating, plunging, pitching, twisting and flapping motions of a finite aspect-ratio wing. M. Radmanesh *et al.* (2014) designed a novel simple strategy to choose and accommodate an airfoil based on the effects of airfoil type and plan-form shape on the flight performance of a micro air vehicle by studying its unsteady aerodynamics.

A. Shokrgozar *et al.* (2016) studied the 3D axisymmetric unsteady stagnation-point flow and heat transfer impinging on a flat plate when the plate is moving with variable velocity and acceleration towards the main stream or away from it.

Husain, Abdullah and Yap (33) did a two-dimensional analysis of tandem/staggered arranged airfoils of the canard and wing of an Eagle 150 aircraft using computational fluid dynamics and also conducted aerodynamic tests in an open-circuit wind tunnel.

In this work, an in-depth study is undertaken to understand the effect of two airfoils exhibiting unsteady motion on each other, the change in circulation, the motion of the trailing edge vortices and their effect on the airfoils. The aerodynamic characteristics are scrutinized, for example the C_l vs α plot is scrutinized to see what causes a spike, the corresponding change in induced drag, location of the trailing edge vortex shed from the leading wing and the change in circulation.

2. NUMERICAL PROCEDURE

The current numerical method consists of extending an unsteady analysis of a single airfoil and its wake using discrete vortices proposed by Katz (2001) to include multiple airfoils and hence multiple wakes. The airfoils are simulated using a discrete lumped vortex model, where the zero-normal boundary condition is applied on the actual camberline. Each of the multiple unsteady wakes is simulated using trailing edge discrete vortices shed from the airfoils at every time-step as shown schematically in Fig. 1a. The flow field is force-free and the strength of the wake vortices remains unchanged. However, the location of the free vortices is updated every time instant using a time-stepping method. The presence of multiple airfoils results in two types of numerical singularities: (a) Free wake vortices interact and come infinitesimally close to each other. A vortex core approach proposed by Chorin (1973) is used to prevent such a scenario. (b) Free wake vortices inter-act and come infinitesimally close to the airfoils. When this happens the vortices would be expected to dissipate. However, since a potential flow solution is used here, vortex dissipation is accounted for using a separate near-field vortex-solid surface criterion.

2.1 Unsteady Discrete Vortex Model

An unsteady discrete vortex model is developed starting with potential flow on which corrections for vortex dissipation are imposed and time-looping is employed to evaluate the time instant behaviour of the vortices being shed into the flow field.

Flow past two airfoils in configuration is considered and the camberline of each airfoil is discretised into segments, on which lumped vortices are distributed. On each segment a lumped vortex element is located at the quarter chord and a collocation point, where the 'zero normal flow on a solid surface' boundary condition shown in Eq. (2) is satisfied is located at the three-quarter chord as shown in Fig. 1a schematically. For example, the velocity induced by a lumped vortex element of circulation, Γ located at (x_o, z_o), at an arbitrary point, $P(x, z)$ are given as in Eq. (1):

$$u = \frac{\Gamma}{2\pi}\frac{z - z_o}{(x - x_o)^2 + (z - z_o)^2}$$
$$w = \frac{\Gamma}{2\pi}\frac{x - x_o}{(x - x_o)^2 + (z - z_o)^2} \quad (1)$$

Surface normals as shown in Fig. 1a are generated at the collocation points and the zero-normal flow boundary condition is satisfied at the collocation points on the actual camberline of the airfoil and not on the chord line. For a different angle of attack, the influence coefficients are generated by using an updated definition of the surfaces normals and the segment definitions are not re-generated.

An unsteady solution involves accounting for the change in circulation of the lifting surfaces at every instant of time and hence update the strength of the bound vortices of the lumped vortices given in Eq. (1). This change in circulation is due to the change in the strength of the bound vortices as well as the induced velocities due to the free wake vortices shed by both airfoils.

For example, at time-step = 1, a single wake vortex of strength $\Gamma^A_{w,1}$ is shed behind airfoil A and another single wake vortex of strength $\Gamma^B_{w,1}$ is shed behind airfoil B as shown in Fig. 1c. Therefore, at time-step = 1, the strength of the bound vortices on both airfoils is affected by $\Gamma^A_{w,1}$ and $\Gamma^B_{w,1}$.

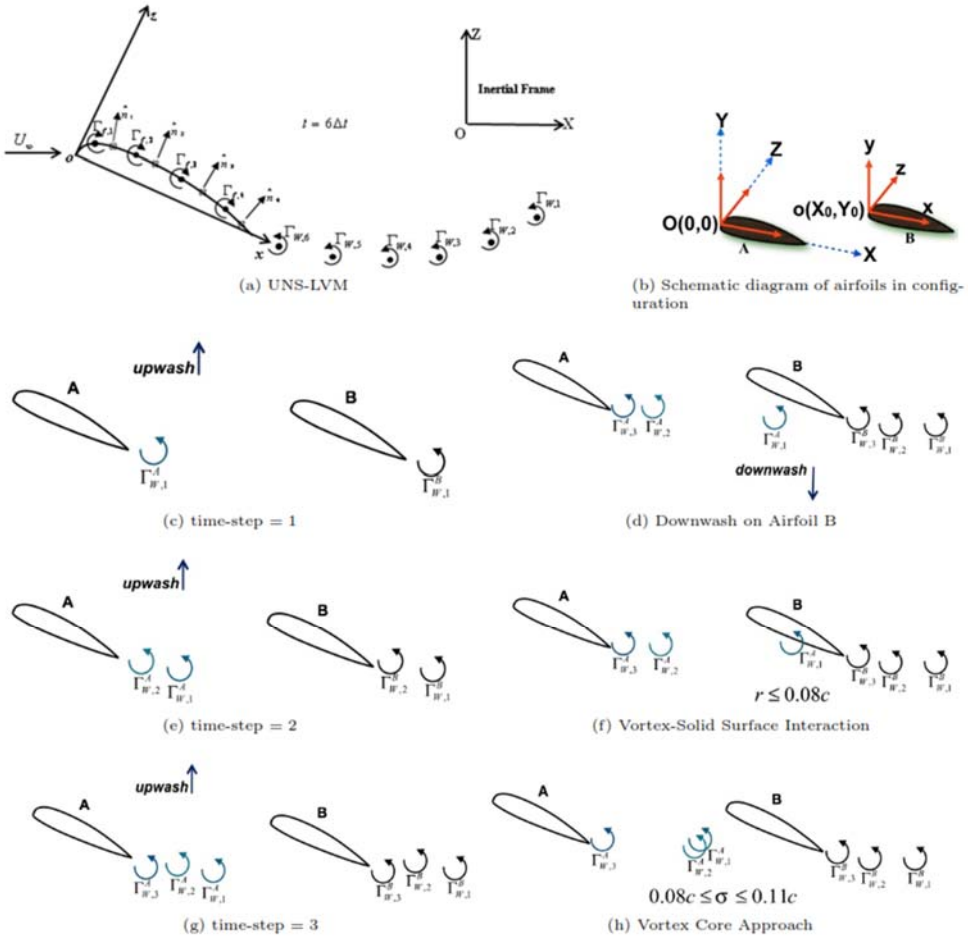

(a) UNS-LVM
(b) Schematic diagram of airfoils in configuration
(c) time-step = 1
(d) Downwash on Airfoil B
(e) time-step = 2
(f) Vortex-Solid Surface Interaction
(g) time-step = 3
(h) Vortex Core Approach

Fig. 1. Unsteady Lumped Vortex Model.

At time-step = 2, $\Gamma^{A}_{w,1}$ and $\Gamma^{B}_{w,1}$ move along with the free stream making way for a new set of single wake vortices of strength $\Gamma^{A}_{w,2}$ and $\Gamma^{B}_{w,2}$, which are shed be-hind airfoils A and B respectively, as shown in Fig. 1e. Therefore, at time-step = 2, the strength of the bound vortices on both airfoils is affected by $\Gamma^{A}_{w,1}$, $\Gamma^{B}_{w,1}$, $\Gamma^{A}_{w,2}$ and $\Gamma^{B}_{w,2}$

At time-step = 3, $\Gamma^{A}_{w,1}$, $\Gamma^{B}_{w,1}$, $\Gamma^{A}_{w,2}$ and $\Gamma^{B}_{w,2}$ move along with the free stream making way for a new set of single wake vortices of strength $\Gamma^{A}_{w,3}$ and $\Gamma^{B}_{w,3}$, which are shed behind airfoils A and B respectively, as shown in Fig. 1g. Therefore, at time-step = 3, the strength of the bound vortices on both airfoils is affected by, $\Gamma^{A}_{w,1}$, $\Gamma^{B}_{w,1}$, $\Gamma^{A}_{w,2}$, $\Gamma^{B}_{w,2}$, $\Gamma^{A}_{w,3}$ and $\Gamma^{B}_{w,3}$ It is to be noted that if any of the vortices shed from airfoil A, say Γ , 1 is ahead of the leading edge of air-foil B, it causes an upwash or enhances lift as shown in Figs 1c, 1e and 1g. On the other hand, if it crosses the leading edge of airfoil B, it causes a downwash or loss in lift as shown in Fig. 1d.

Kelvin condition is satisfied as shown in Eq. (3). Hence, at every time instant, the strength of the free wake vortices shed from earlier time-steps are known and the free wake vortex shed in that particular time instant is calculated using the Kelvin condition. The strength of the wake vortices already shed does not change but their positions are updated at every time instant.

Therefore, the unsteady discrete vortex model satisfies the Laplace equation or a steady-state potential flow solution at every instant of time, using updated values of the strength of the bound vortices.

2.2 Boundary Conditions and Influence coefficients

By definition, the Kutta condition is satisfied by the lumped vortex elements and it is not included into the solution explicitly. The unknowns in this method are the strengths of the bound vortices of the two airfoils (2N in number) and the strengths of the most latest shed trailing vortices (2 in number) from the two air-foils.

Boundary conditions imposed are the zero-normal flow on a solid surface boundary condition given in Eq. (2), which accounts for the strengths of the bound vortices and the Kelvin condition given in Eq. (3), which ac-counts for the strengths of the latest shed trailing vortices for each airfoil in the configuration. Both these conditions are used in tandem at every time instant to generate the (2N + 2) × (2N + 2) influence coefficient matrix for the two airfoils in configuration, where N is the number of discrete vortices used to simulate each airfoil. Finally, a matrix equation given in Eq. (4) is solved at every time instant for the strength of the bound vortices of each airfoil (ΓN) in the configuration and the strength of the latest wake vortices shed from each airfoil (Γw,t). The subscript t denotes the latest time step.

Then, F1ΓA is the influence of the bound vortices of airfoil A on itself. F1ΓB is the influence of the bound vortices of airfoil B on airfoil A. G1ΓA is the influence of the bound vortices of airfoil A on airfoil B. G2ΓB is the influence of the bound vortices of airfoil B on itself. ΓWA and ΓWB are the strengths of the latest shed trailing vortices from airfoil A and B respectively. F3ΓWA is the influence of the latest shed trailing vortex from airfoil A on airfoil A. F4ΓWB is the influence of the latest shed trailing vortex from airfoil B on airfoil A. G3ΓWA is the influence of the latest shed trailing vortex from airfoil A on airfoil B. G4ΓWB is the influence of the latest shed trailing vortex from airfoil B on airfoil B. The first two rows of the influence coefficient matrix are a statement of the zero-normal flow boundary condition on both the airfoils.

The last two rows of the influence coefficient matrix are a statement of the Kelvin condition on both the airfoils individually.

$$(\nabla\Phi + U_\infty)\hat{n} = 0; \qquad \hat{n} = \hat{n}(X,Y,Z,t) \tag{2}$$

$$\frac{d\Gamma}{dt} = \frac{d\Gamma_f(t)}{dt} + \frac{d\Gamma_w}{dt} = 0 \tag{3}$$

$$\begin{pmatrix} F1 & F2 & F3 & F4 \\ G1 & G2 & G3 & G4 \\ L1 & L2 & L3 & L4 \\ M1 & M2 & M3 & M3 \end{pmatrix} \begin{pmatrix} \Gamma_A \\ \Gamma_B \\ \Gamma_{WA} \\ \Gamma_{WB} \end{pmatrix} = \begin{pmatrix} (rhs)_A \\ (rhs)_B \\ -\left(\Gamma_{WA+1} + \Gamma_{WA+2} + ...\right) + \Gamma_{WA,t-1} \\ -\left(\Gamma_{WB+1} + \Gamma_{WB+2} + ...\right) + \Gamma_{WB,t-1} \end{pmatrix} \tag{4}$$

where

$$F1 = \begin{pmatrix} f_{1,1} \vdots f_{1,N} \\ \vdots\vdots\vdots \\ \vdots\vdots\vdots \\ f_{N,1} \vdots f_{N,N} \end{pmatrix}_{N\times N} \qquad F2 = \begin{pmatrix} f_{1,N+1} \vdots f_{1,2N} \\ \vdots\ \vdots\ \vdots \\ \vdots\ \vdots\ \vdots \\ f_{N,N+1} \vdots f_{N,2N} \end{pmatrix}_{N\times N}$$

$$F3 = \begin{pmatrix} f_{1,2N+1} \\ \vdots \\ \vdots \\ f_{N,2N+1} \end{pmatrix}_{N\times 1} \qquad F4 = \begin{pmatrix} f_{1,2N+2} \\ \vdots \\ \vdots \\ f_{N,2N+2} \end{pmatrix}_{N\times 1}$$

$$F1 = \begin{pmatrix} g_{N+1,1} \vdots g_{N+1,N} \\ \vdots\ \vdots\ \vdots \\ \vdots\ \vdots\ \vdots \\ g_{2N,1} \vdots g_{2N,N} \end{pmatrix}_{N\times N} \qquad \Gamma_A = \begin{pmatrix} \Gamma_1 \\ \vdots \\ \vdots \\ \Gamma_N \end{pmatrix}_{N\times N}$$

$$G2 = \begin{pmatrix} g_{N+1,N+1} \vdots g_{N+1,2N} \\ \vdots\ \vdots\ \vdots \\ \vdots\ \vdots\ \vdots \\ g_{2N,N+1} \vdots g_{2N,2N} \end{pmatrix}_{N\times N} \qquad \Gamma_B = \begin{pmatrix} \Gamma_{N+1} \\ \vdots \\ \vdots \\ \Gamma_{2N} \end{pmatrix}_{N\times 1}$$

$$G3 = \begin{pmatrix} g_{N,2N+1} \\ \vdots \\ \vdots \\ g_{2N,2N+1} \end{pmatrix}_{N\times 1} \qquad G4 = \begin{pmatrix} g_{N+1,2N+2} \\ \vdots \\ \vdots \\ g_{2N,2N+2} \end{pmatrix}_{N\times 1}$$

$$\Gamma_{WA} = (\Gamma_{WA,t})_{N\times 1} \qquad \Gamma_{WB} = (\Gamma_{WB,t})_{N\times 1}$$

$$L1 = M2 = (1...1)_{1\times N} \qquad L2 = M1 = (0...0)_{1\times N}$$

$$L3 = M4 = (1)_{1\times N} \qquad L4 = M3 = (0)_{1\times N}$$

The pressure difference between the upper and lower surfaces of an airfoils j^{th} element is given as:

$$\Delta p_j = \rho\left[(U(t)+u_W, W(t)+w_W)_j.\tau_j \frac{\Gamma_j}{\Delta l_j}\right] + \rho\frac{\partial}{\partial t}\int_0^{x_j}\gamma(x_0,t)dx_0$$

$$or \quad \Delta p_j = \rho\left[(U(t)+u_W, W(t)+w_W)_j.\tau_j \frac{\Gamma_j}{\Delta l_j}\right] + \rho\frac{\partial}{\partial t}\Gamma(x_j,t)$$

$$or \quad \Delta p_j = \rho\left[(U(t)+u_W, W(t)+w_W)_j.\tau_j \frac{\Gamma_j}{\Delta l_j}\right] + \rho\frac{\partial}{\partial t}\sum_{k=1}^{j}\Gamma_k$$

Where, $U(t)$ and $W(t)$ are the components of the free stream velocity, u_W and w_W are the velocity components induced by the wake vortices on the airfoil, τ_j is the unit vector tangential to the surface of segment j of the airfoil, Γ_j is the strength of the bound vorticity on segment j.

As seen above, the first two terms in the expression for pressure are for the steady state case. The second unsteady term is due to the accelerated flow and also contributes to the pressure difference. This first order time derivative is calculated as:

$$\frac{\partial}{\partial t}\Gamma(x_j,t) = \frac{\Gamma(x_j,t_2)-\Gamma(x_j,t_1)}{\Delta t}$$

$$= \sum_{k=1}^{j}\frac{\Gamma(x_k,t_2)-\Gamma(x_k,t_1)}{\Delta t}; \quad \Delta t = t_2 - t_1$$

Hence, the aerodynamic loads are as follows. 1. Lift

$$L = \int_0^x (\Delta p)\cos\alpha dx = \sum_{j=1}^{N} \Delta p_j \Delta l_j \cos\alpha_j$$

$$= \rho\int_0^x (U(t)+u_w, W(t), w_W)_j . \tau_j \frac{\Gamma_j}{\Delta l_j}\cos\alpha dx$$

$$+ \rho\frac{\partial}{\partial t}\int_0^{x_j} \gamma(x_0,t)dx_0 \cos\alpha dx$$

2. Induced Drag

$$D = \int_0^x (\Delta p)\sin\alpha dx = \sum_{j=1}^{N} \Delta p_j \Delta l_j \cos\alpha_j$$

$$= \rho\int_0^x (U(t)+u_w, W(t), w_W)_j . \tau_j \frac{\Gamma_j}{\Delta l_j}\sin\alpha dx$$

$$+ \rho\frac{\partial}{\partial t}\int_0^{x_j} \gamma(x_0,t)dx_0 \sin\alpha dx$$

3. Pitching Moment about the Leading Edge of the airfoil

$$M_0 = -\sum_{j=1}^{N} \Delta p_j \cos\alpha_j \Delta l_j x_j$$

Where α is the angle between free stream velocity and the unit normal to the segment *j*.

Hence, the aerodynamic coefficients are:

$$C_l = \frac{L}{\frac{1}{2}\rho U_\infty^2 c}, \quad C_{di} = \frac{D}{\frac{1}{2}\rho U_\infty^2 c}, \quad C_m = \frac{M_0}{\frac{1}{2}\rho U_\infty^2 c}$$

2.3 Near-Feld Vortex-solid Surface interaction

With time, the free vortices shed into the wake travel and change their original locations along with the free-stream. A time-stepping method is used to update the location of the shed vortices at the end of each time step. In the current problem since multiple airfoils are present in the flow field, the wake vortices of the leading airfoil interact with the trailing airfoil before travelling with the free-stream as shown in Fig. 1f. Computation-ally, this condition will lead to numerical singularities and physically, it is expected that a free vortex will dissipate when it hits a solid surface. This has been re-ported in literature as well, for example, it was observed by Fage and Johansen (1927) and Nakagawa (1988) that vortices which are too close to the surface of a plate, dissipate by the action of viscosity. In the present work, the effect of dissipation of the vortices is taken into ac-count using the condition given in Eq. (5), where r is the distance between a free vortex in the flow field and a solid surface.

The relation in Eq. (5) is arrived at by conducting numerical tests, which show that if r is greater that 8%chord, the method is unable to capture the unsteady nature of the flow-field accurately. Also, if r is less than 8% chord, say, r = 0.05c, it does not give any additional information about the flow field. Hence, r = 0.08c is used as a cut-off point.

Whenever a wake vortex satisfies this condition, its influence on the flow-field, i.e. the velocity induced by it on the bound vortices, wake vortices and hence, the wake shape is ignored since it is considered dissipated. The strength of this vortex is however continued to be used to satisfy the Kelvin condition even after this condition is met as the flow-field is considered to be force-free and the net vorticity of the flow-field remains constant.

$$r \le 0.08c \tag{5}$$

2.4 Near-Feld Vortex-Vortex Interaction

In the current problem, multiple airfoils shed multiple set of free wake vortices into the flow field, which travel freely with the free-stream and interact with each other. When the distance between two such free wake vortices becomes infinitesimal as shown in Fig. 1h, computation-ally this condition leads to numerical singularities. To counter this condition, a vortex core approach is taken, where a radius σ is scooped out about the vortex and the stream function criteria suggested by Chorin (1973) is used as given in Eq. (6). This prevents any infinite velocities due to two vortices coming too close to each other. In the current work, σ = 0.08c.

$$\Psi_\sigma = \begin{bmatrix} \frac{\Gamma \log r}{2\pi} & r > \sigma; \frac{\Gamma \log\left(\frac{r}{\sigma}\right)}{2\pi} & r \le \sigma \end{bmatrix} \tag{6}$$

Where r is the distance between two free vortices and σ is the radius of the core scooped out about the free vortex. The vortex dissipation criteria in Eq. (5) and vortex core criteria in Eq. (6) depend on the airfoil chord length and in our current study the suitable ranges of r and σ arrived at by inspection are: (7-10)%c. This same value is used for all results generated and for validation.

3. RESULTS

Results are presented for a configuration consisting of two airfoils as shown in Fig. 1b. The leading airfoil is denoted as A and the trailing airfoil is denoted as B. A fixed reference frame, (X, Y) is attached to airfoil A and the origin, O (0, 0) of this reference frame is located at the leading edge of airfoil A. A moving reference frame, (x, y) is attached to the trailing airfoil B and the origin of this reference frame o(X0, Y0) is located at the leading edge of airfoil B. Note that X0 and Y0 are calculated with respect to the fixed reference frame, (X, Y).

3.1 Unsteady Wake Vortices of Tandem Airfoils Set Into Motion with Sudden Acceleration

The $C_l(t)$ from the current work for two NACA0012 airfoils in configuration, each of chord length, c = 1 shown in Fig. 1b is compared with the analytical results of Wagner (1925) for a single airfoil. The airfoils in the present analysis and that of Wagner are at an angle of attack of 5o and set into motion with a sudden acceleration.

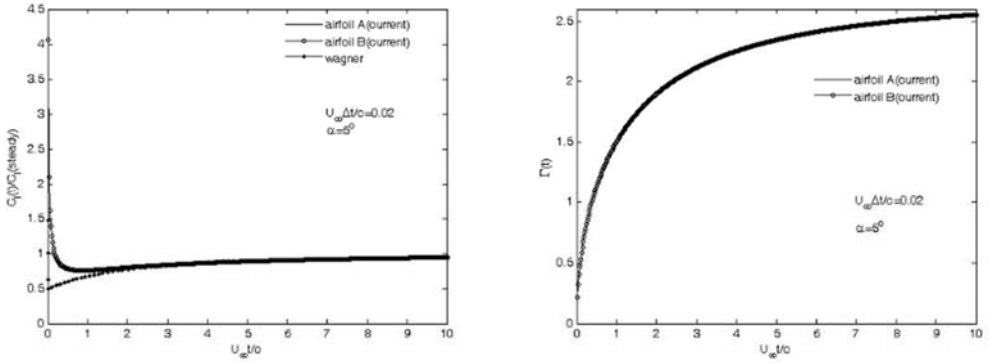

(a) C_l (b) Γ

Fig. 2. Airfoils in Configuration.

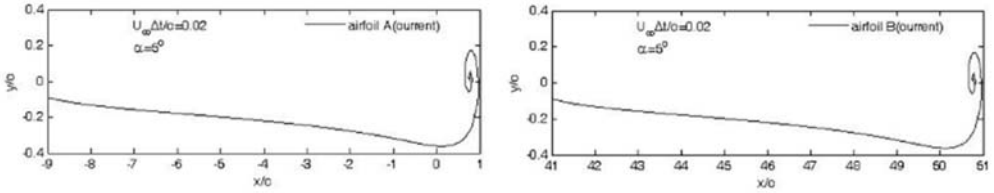

(a) Airfoil A (b) Airfoil B

Fig. 3. Wake Shape.

Since Wagner's analytical result is for a single airfoil, the distance between the two NACA0012 airfoils in the present analysis is taken as 50. It is expected that at such a large distance, the influence of the airfoil bound vortices and the wake vortices on each other will be minimal.

The plot of $\frac{C_l(t)}{C_l(steady)}$ vs $\frac{U_\infty t}{c}$ for both airfoils is shown in Fig. 2a. It is seen that the $\frac{C_l(t)}{C_l(steady)}$ values of both airfoils exactly match each other and the comparison with the analytical result is also good. There is how-ever, some disagreement of the current result with that of Wagner at very small time steps, i.e. $\frac{U_\infty t}{c} \le 1$. This may be attributed to the loss in accuracy due to the constraints of a typical numerical approach and de-creasing the time-step does not improve the result. This problem is not expected in an analytical approach as that of Wagner.

Fig. 2b shows the circulation distribution, $\Gamma(t)$ vs $\frac{U_\infty t}{c}$ and Fig. 3 shows the vortex roll up at $\frac{U_\infty t}{c} = 1$ for both airfoils from the current analysis. As expected the result shows that both airfoils are unaffected by the presence of each other. Results for the circulation and wake shape are not available from Wagner for comparison.

3.2 Wake Vortices set off by Non-Interacting Airfoils Pitching in Tandem

The plot of $C_l - \alpha$ for both airfoils, pitching in tandem for the conditions shown below and as shown in Fig. 4a.

$$\alpha = 3^\circ + 10\sin\omega t, \quad \frac{\omega c}{2U_\infty} = 0.1, \quad \frac{\Delta t U_\infty}{c} = 1$$

The pitch axis is at the quarter chord, $\frac{c}{4}$. The results from the present work are compared with those of Mc-croskey (1981) and Maskew (1988) which are for single airfoils. Hence, the present results are generated for $\frac{d}{c} = 5000$ .It is seen that there is no difference in the performance of both airfoils and they exactly match. They behave like single operating airfoils as they do not interact since the distance between them has been taken to be very large. The comparison with literature is good. The wake shapes can be seen in Fig. 4b and the result emphasizes that the airfoils do not interact given the distance between them.

3.3 Behavior of Wake Vortices of Tandem Non-Interacting Heaving Airfoils

The configuration of two NACA0012 airfoils as shown in Fig. 1b is subjected to heaving motion. Wake shape of both the airfoils predicted using the present numerical method is compared with the computational and experimental results of Katz and Weihs (1978) for a single airfoil. In this case too, since the results of Katz and Weihs are for a single airfoil, the distance between the two airfoils in configuration is taken as 100*c*. It is expected that at such a large distance, the influence of the airfoil

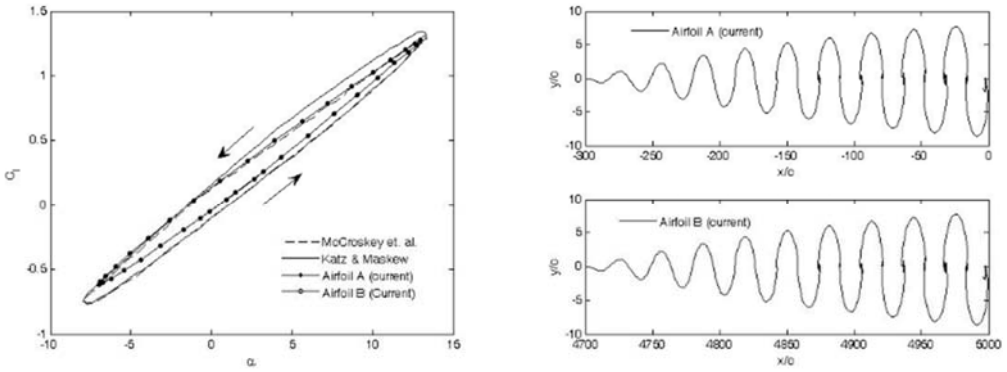

(a) $C_l(t)$ (b) $WakeShape$

Fig. 4. Airfoils Pitching in Configuration.

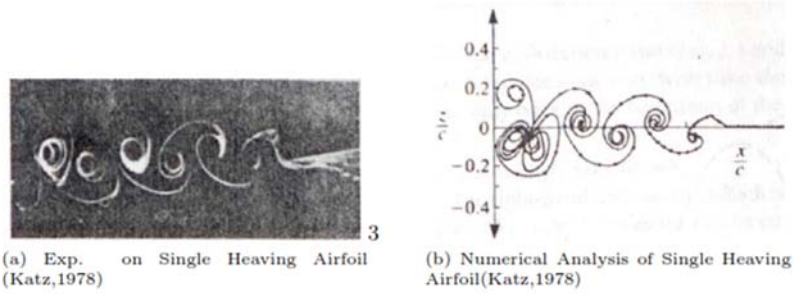

(a) Exp. on Single Heaving Airfoil (Katz,1978) 3

(b) Numerical Analysis of Single Heaving Airfoil(Katz,1978)

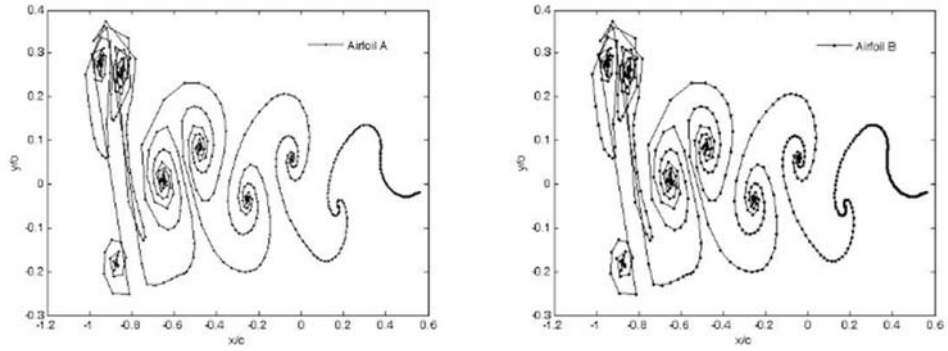

(c) Leading airfoil in a configuration from Current Work (d) Trailing airfoil in a configuration from Current Work

Fig. 5. Wake of Single and Tandem Heaving Airfoils.

bound vortices and the wake vortices on each other will be minimal. The parameters of heaving motion are as follows:

$$\frac{\omega c}{2U_\infty} = 8.5; \frac{\Delta t U_\infty}{c} = 1.56 / s; \frac{h_o}{c} = 0.019; \omega = 26.77^c / s$$

The experimental and numerical results of Katz and Weihs are shown in Figs. 5a and 5b respectively. The wake shape from the current analysis for both airfoils are shown in Figs. 5c and 5d. It can been seen that there is no interaction between the airfoil bound vortices and wake vortices due to the 100c distance between them and hence the wake shape of both airfoils are not different from each other.

3.4 Effect of Trailing Edge Vortices on the Performance of Interacting Tandem Airfoils

A comparison between the results from the present study and the computational results of Platzer (1993) for airfoil and wake interaction is presented here. For a configuration of two NACA0012 airfoils, $(X_o, Y_o) = (0.5c, 0.2c)$, Platzer's numerical code could not account for the interaction of the vortices shed from the leading airfoil with the trailing airfoil surface for such minimal distances. They had to therefore adjust the configuration in such a way that the vortices do interact but they do not come close enough to induce infinite velocities in the numerical

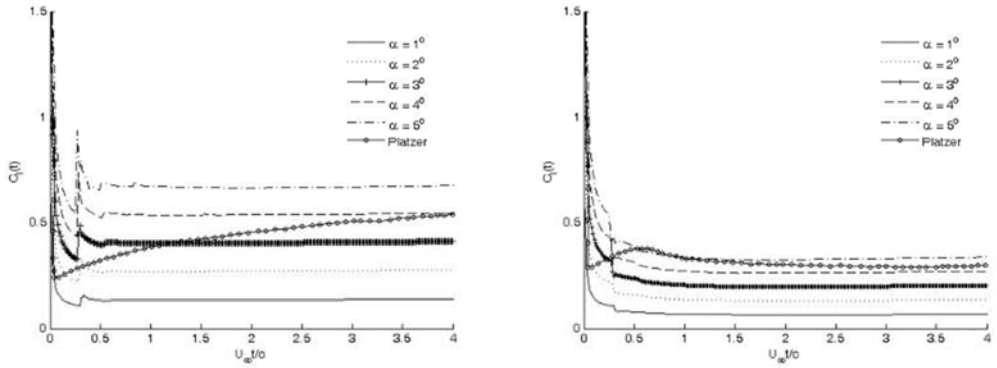

(a) $C_l(t)$ of Leading Airfoil (b) $C_l(t)$ of Trailing Airfoil

Fig. 6. Tandem Airfoils Interacting with their Wakes.

solution. Hence, they used the con-figuration $(X_o, Y_o) = (0.5c, 0.2c)$ where the airfoils are also undergoing a step change in angle of attack from 0° to 5°.

The results for this configuration without the step change in angle of attack is generated with the present code and presented in Fig. 6. The results show individual cases of different angles of attack for the airfoils in configuration. The present numerical scheme accounts for the interaction of vortices with solid airfoil surfaces as well as with each other at minimal distances without inducing any infinite velocities in the flow-field. Sharp changes in $C_l(t)$ for $\frac{U_\infty t}{c} \approx 0.3$ are observed for both airfoils. For the leading airfoil, the 'cusp' of C_l increases with increase in the angle of attack. In other words, the C_l drops to a minimum and then sees a sudden jump at $\frac{U_\infty t}{c} \approx 0.3$. For the trailing airfoil, the C_l decreases but less than the leading airfoil and at $\frac{U_\infty t}{c} \approx 0.3$, it drops sharply. The drop in C_l of airfoil A can be attributed to the fact that the strength of the trailing edge vortex shed by the leading airfoil A and the corresponding downwash caused by it on itself increases with the increase in its angle of attack. The same trailing edge vortex shed from airfoil A initially causes an upwash and hence an increase in C_l of the trailing airfoil B. Essentially, for $0 < \frac{U_\infty t}{c} \le 0.3$, the effect of this trailing edge vortex on both airfoils takes precedence over the effect of angle of attack of the individual airfoils.

However, at $\frac{U_\infty t}{c} \approx 0.3$, the trailing edge vortex just crosses the leading edge of airfoil B. At this point, airfoil A sees a sharp spike in its C_l as now the upwash of airfoil B and the effect of its own angle of attack dominates. This sharp spike in Cl of airfoil A causes a corresponding large downwash on airfoil B, which therefore sees a sharp decrease in its C_l.

The effect of the strong trailing vortex shed by airfoil A wanes with increasing distance. In this case, it is seen that the effect is minimum at $\frac{U_\infty t}{c} \approx 0.3$. After this, the effect of the angle of attack of individual airfoils and their effect on each other (i.e. the downwash of airfoil A on airfoil B and upwash of airfoil B on airfoil A) take precedence. Platzer's results on the other hand are similar to that of a single airfoil case of Wagner shown in Fig. 2.

3.5 Effect of Relative Velocity of Tandem Airfoils on Wake Vortices

As seen earlier, the effect of the trailing vortices wanes with increasing distance from the airfoils. In this case, the leading airfoil A is set into motion with sudden acceleration with a velocity of $V_A = 15m/s$. The trailing airfoil is also set into motion with a sudden acceleration but with a finite relative velocity with respect to airfoil A. Three such velocities are considered, namely, $V_B = 20, 25, 30 m/s$. The starting location of the leading edge of the trailing airfoil B is $o(X_o, Y_o) = (6c, c)$ and both airfoils are at an angle of attack, $\alpha_A + \alpha_B = 3^\circ$. The origin $O(0, 0)$ is located at the leading edge of the leading airfoil A.

The C_l of airfoil A shown in Fig. 7a, which consists of three peaks and three troughs corresponding to the relative velocities of $V_B - V_A = 5, 10, 15 m/s$. The highest and sharpest peak corresponding to the maximum relative velocity of 15*m/s* occurs first at $\frac{U_\infty t}{c} \approx 4$ and the lowest and least sharp peak corresponding to the mini-mum relative velocity of 5*m/s* occurs last at $\frac{U_\infty t}{c} \approx 14$. Given that the C_l is calculated using the instantaneous circulation, the sharp peaks and troughs mean that $\frac{d\Gamma}{dt}$ is significant.

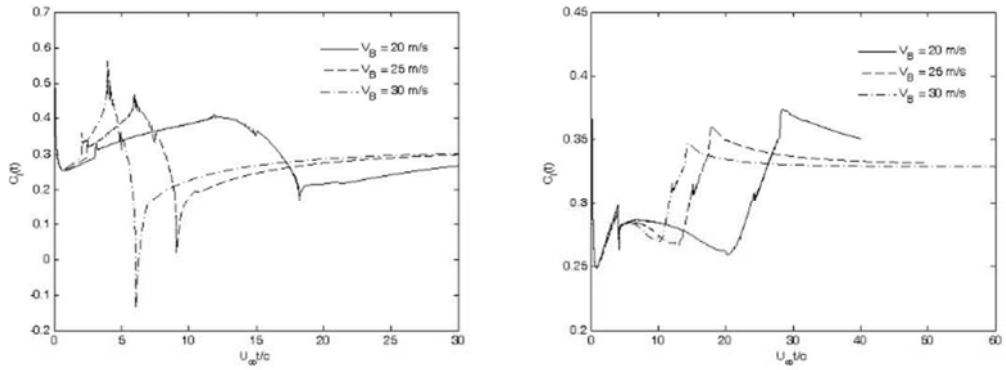

(a) Airfoil A (b) Airfoil B

Fig. 7. Airfoils with Relative velocity: Cl.

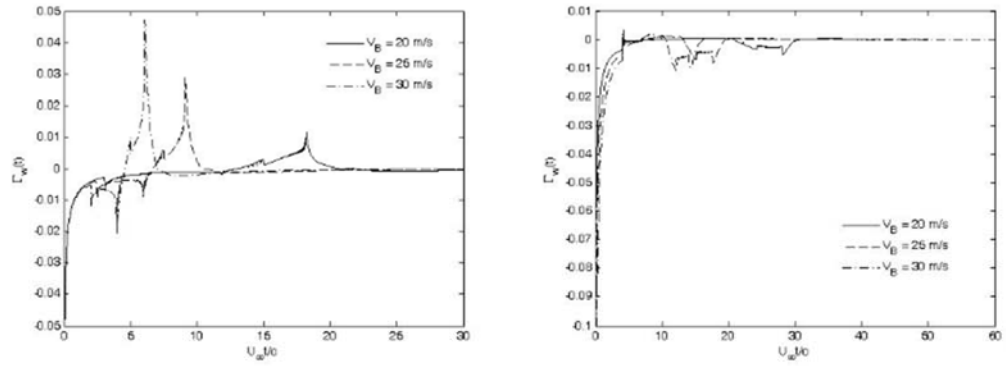

(a) Airfoil A (b) Airfoil B

Fig. 8. Airfoils with Relative velocity: wake strength.

This shows up in the C_l plot, especially for the relative velocities of 10 and 15*m/s,* where there are significant C_l maxima and minima.

For airfoil B, three cusps in the C_l are seen corresponding to the three relative velocities as shown in Fig. 7b. Again, the large values of dΓ show up in the C_l plot of dt airfoil B as maxima and minima points.

The evolution of the strength of the wakes with time is shown in Fig. 8.

Corresponding to the increasing C_l , the induced drag also increases as seen in Fig. 9a but around $\frac{U_\infty t}{c} \approx 6$, when the C_l sees a sharp drop, the induced drag also sees a sharp drop. These lowest induced drag points mean that at this point the airfoil is experiencing a forward thrust, which increases with increase in relative velocity.

This can be explained further with the help of Fig. 10, where the locations of the three 'kinks' in the C_l plot corresponding to the relative velocity 5*m/s* are marked in Fig. 10a. The corresponding relative distances be-tween the airfoils is shown in Fig. 10b. It can be seen from Fig. 10a that for the 'kink' located at A, the corresponding relative distance is ≈ 3 as shown in Fig. 10b. A schematic of the location of the two airfoils in this position is shown in Fig. 10c. Similarly, for the location B, the relative distance is 1, which means that the air foils are 'bumper to bumper' as schematically shown in Fig. 10d. For position C, the relative distance is zero, which means that the leading edges line up as shown in Fig. 10e. Such 'kinks' in the C_l plot are also present for the relative velocities of 10 and 15*m/s* and can be explained the same way.

It can also be seen from Fig. 7 that till $\frac{U_\infty t}{c} \approx 2$ the curves merge but after this time, the slopes become different for different relative velocities. In other words, slopes increase with increase in relative velocity. For example, for the curve corresponding to a relative velocity of 15*m/s*, the C_l increases till $\frac{U_\infty t}{c} \approx 4$. During this time, it can be seen from Fig. 8a, the trailing edge vortex has negative strength, which causes an upwash and hence an increased C_l . Around $\frac{U_\infty t}{c} \approx 4$, however, the strength sees a sharp

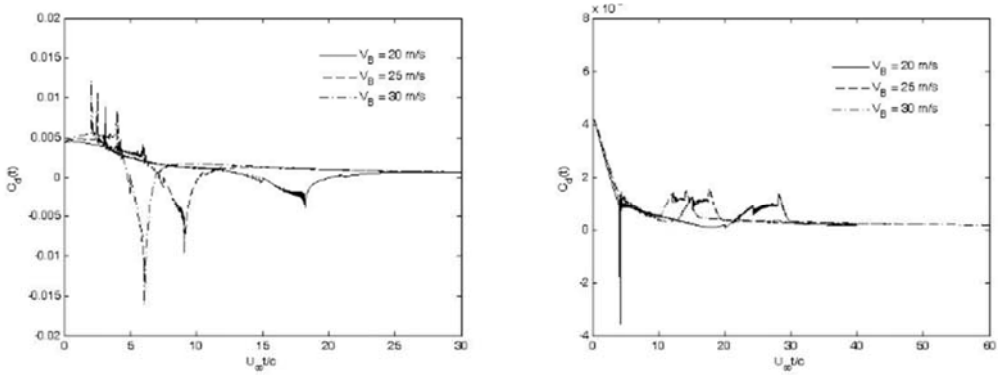

(a) Airfoil A (b) Airfoil B

Fig. 9. Airfoils with Relative velocity: C_d .

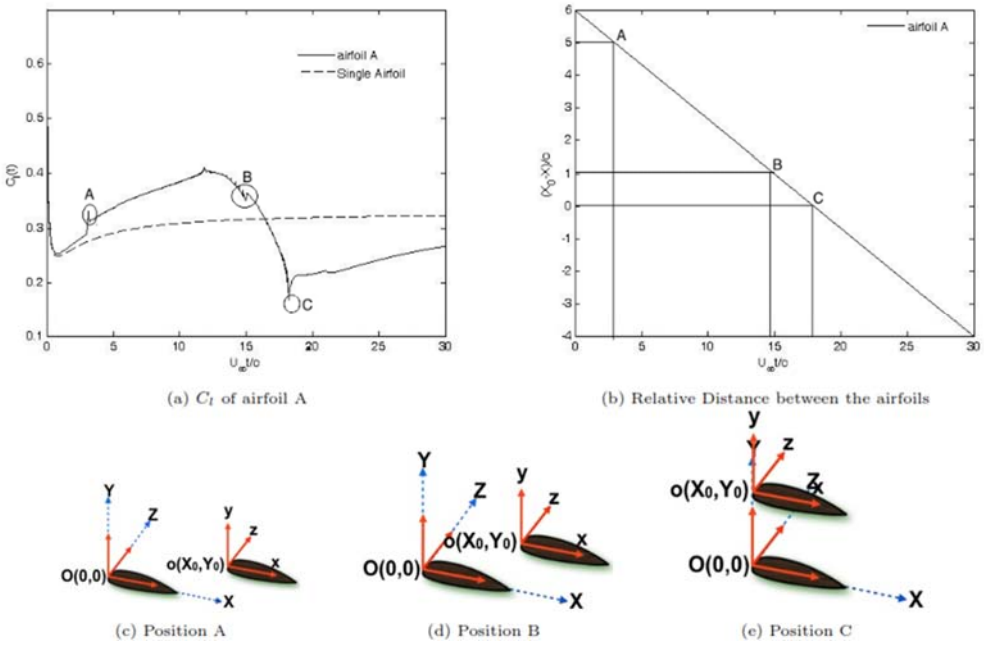

(a) C_l of airfoil A (b) Relative Distance between the airfoils

(c) Position A (d) Position B (e) Position C

Fig. 10. V_A = 15m / s, V_B = 20m / s .

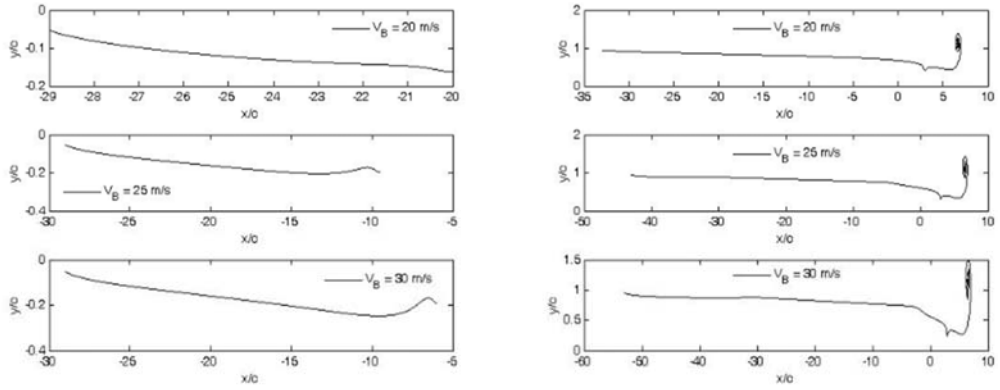

(a) Airfoil A (b) Airfoil B

Fig. 11. Airfoils with Relative velocity: wake shape.

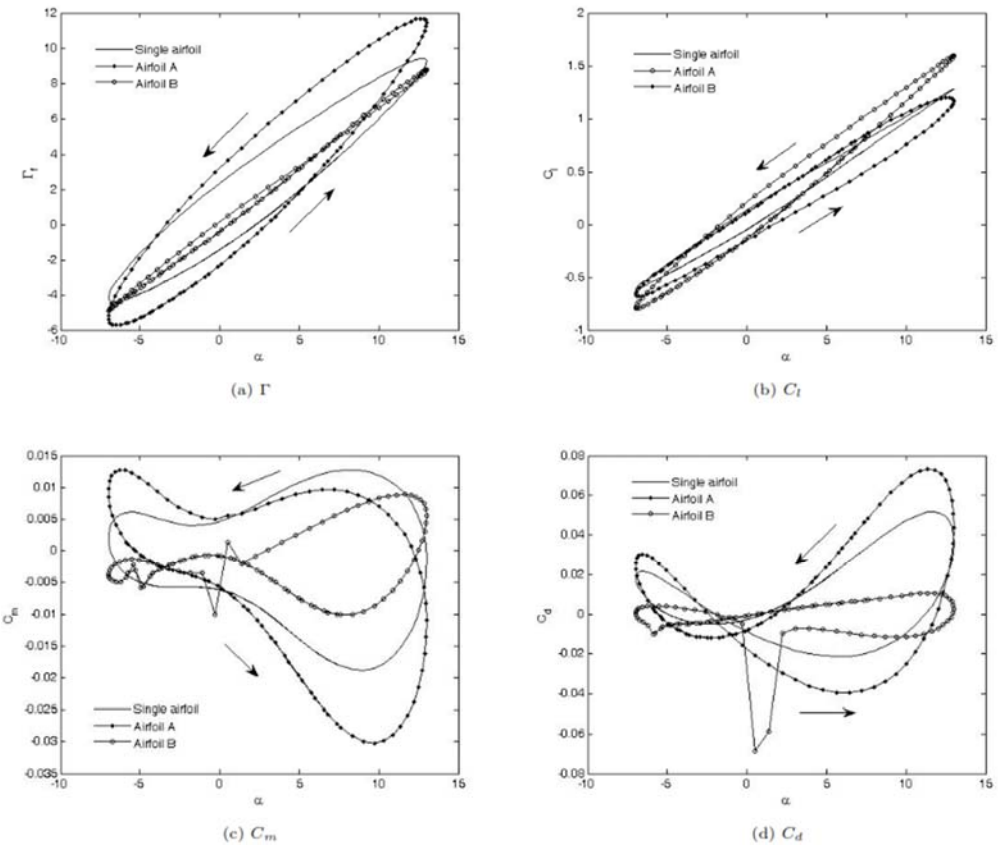

Fig. 12. Pitching: Tandem Airfoils vs Single Airfoil.

positive spike which reaches a maximum at $\frac{U_\infty t}{c} \approx 6$. It is at this time, the C_l also sees a sharp drop since now the trailing edge vortex causes a large downwash on the airfoil. At this time the airfoils are in position B shown in Fig. 10d. Soon after this, the trailing edge vortex 'dies' as shown by its zero strength in Fig. 8a. Therefore, the airfoils are now dominated by themselves and not the trailing vortex. It is seen from Fig. 11a that the wake is not significant for airfoil A but there is a significant roll-up of the wake vortices for the trailing airfoil B with the traces of a secondary roll-up as well.

3.6 Single Airfoil and Configuration of Two Airfoils: A Comparative Study of their Pitching Motion

Since the flow field around a single airfoil is different when it is in a configuration with another airfoil, it is expected that there will be differences in their aerodynamic characteristics as well. Hence, a comparison of the same for both airfoils pitching is presented here for the following operating conditions. The pitch axis is at the quarter chord, $\frac{c}{4}$. Additionally, for the tandem airfoils, $\frac{d}{c} = 1.5$.

$$\alpha = 3^\circ + 10\sin\omega t, \frac{\omega c}{2U_\infty} = 0.1; U_\infty = 15m/s; \omega = 3^c/s$$

It is seen from Figs 12a and 12b that compared to the single airfoil, the leading airfoil in the configuration generates greater circulation, $\Gamma(t)$ and corresponding greater $C_l(t)$ for the cycle starting at $\alpha = 5^\circ$, reaching a maximum of $\alpha \approx 13^\circ$ and cycling back to $\alpha \approx -5^\circ$. Both the leading and single airfoils have the same starting $\Gamma(t)$ and $C_l(t)$ as expected at $\alpha = 5^\circ$. The trailing airfoil, on the other hand, has a greater starting $\Gamma(t)$ and $C_l(t)$ at $\alpha = 5^\circ$ compared to both the single and leading airfoils. However, it generates lesser $\Gamma(t)$ and corresponding lesser $C_l(t)$ during the cycle between $\alpha \approx 10^\circ$ and $\alpha = -5^\circ$ compared to both the single and leading airfoils. The hysteresis in $\Gamma(t)$ as well as $C_l(t)$ is much larger for the leading airfoil than the trailing airfoil. In fact, for the trailing airfoil, the hysteresis is almost negligible.

It is also seen from Figs 12c and 12d that around $\alpha = -6^\circ$ and $\alpha = 1^\circ$ there are abrupt changes in the coefficients of pitching moment, C_m and induced drag, C_d for the trailing airfoil B. This can be

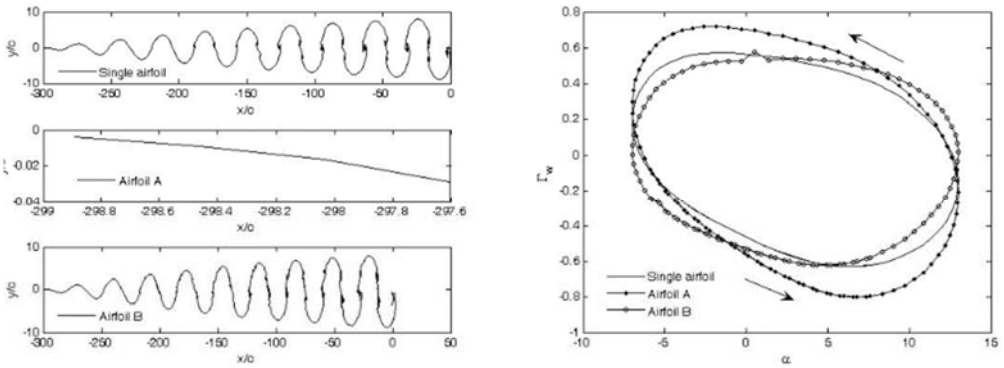

(a) Wake Shape (b) Wake Strength

Fig. 13. Pitching: Tandem Airfoils vs Single Airfoil, Wake.

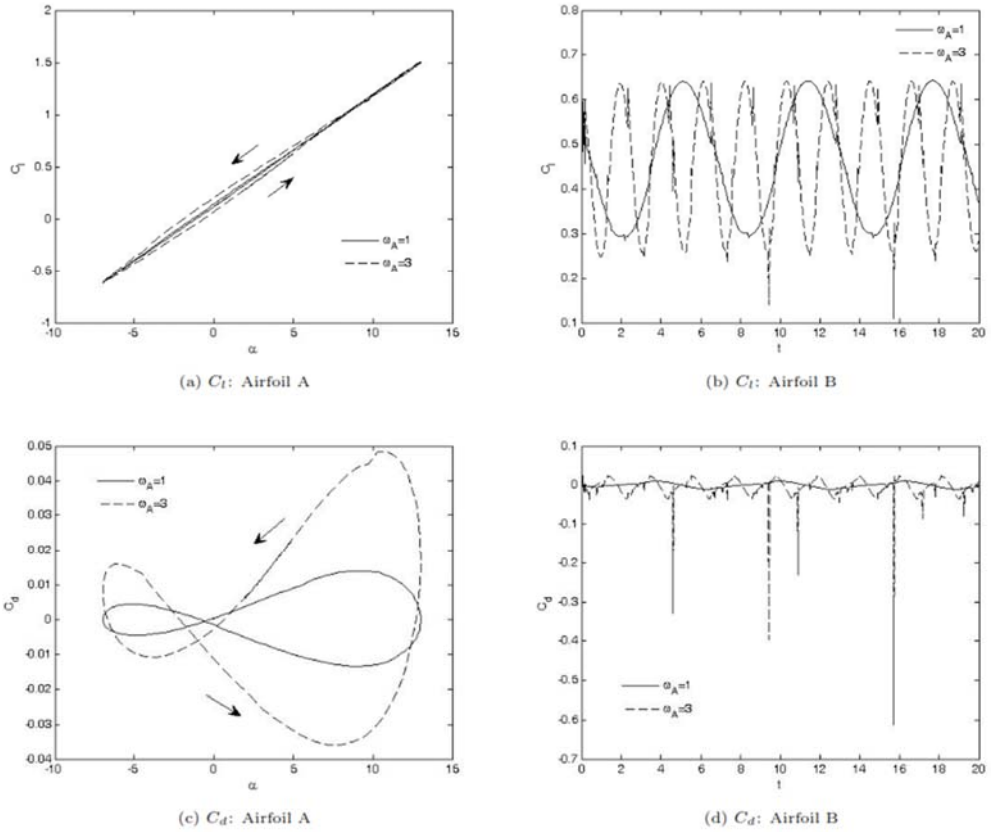

(a) C_l: Airfoil A (b) C_l: Airfoil B

(c) C_d: Airfoil A (d) C_d: Airfoil B

Fig. 14. Only Leading Airfoil Pitching: C_l and C_d.

explained using Fig. 13b as follows.

It is seen in Fig. 13b that for $\alpha \approx -6^{\circ}$, there is a slight increase in $\Gamma_w(t)$, which is the strength of the trailing vortex of airfoil B. The strength is still negative, which indicates that the sense of the vortex is counter-clockwise. This increase in strength of $\Gamma_w(t)$ causes additional downwash on airfoil B, which is an additional vertical component of velocity in the direction opposite to lift, i.e. downwards. This causes a decrease in the effective angle of attack, α at $\alpha \approx -6^{\circ}$ and hence a decrease in $C_l(t)$ as seen in 12b, which in turn causes a decrease in the nose-down or negative $C_m(t)$ as seen in 12c and a corresponding decrease in the induced drag $C_d(t)$ as seen in 12d.

At $\alpha \approx 1^{\circ}$ as seen in Fig. 13b there is a slight increase in the positive or clockwise $\Gamma_w(t)$. This causes an upwash on airfoil B, which is an additional vertical component of velocity in the direction of lift, i.e.

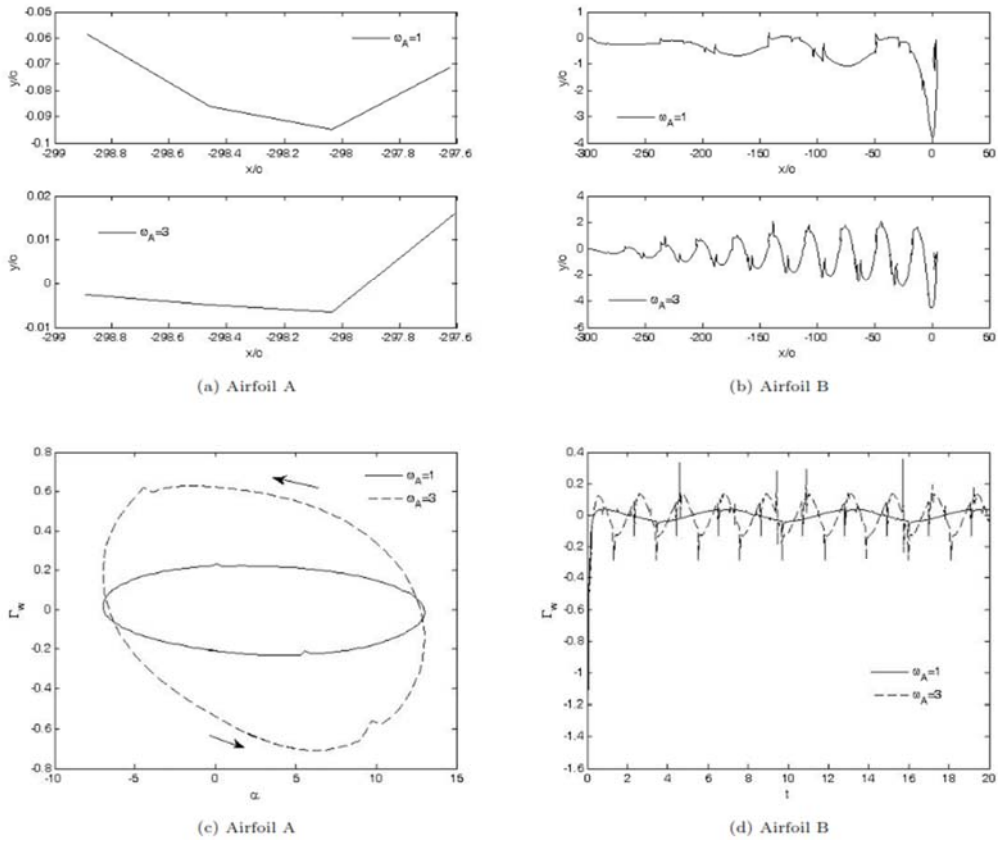

(a) Airfoil A (b) Airfoil B

(c) Airfoil A (d) Airfoil B

Fig. 15. Only Leading Airfoil Pitching: wake strength and roll-up.

upwards. This causes an increase in the effective angle of attack, α at $\alpha \approx 1^{\circ}$ and hence an increase in its $C_l(t)$ as seen in 12b, a corresponding increase in the nose-down or negative $C_m(t)$ as seen in 12c and a large increase in the negative $C_d(t)$ as seen in 12d.

It is seen from 12d that unlike airfoil A and the single airfoil, the $C_d(t)$ of airfoil B hovers around zero and negative even for $\alpha=12^{\circ}$, which is a post-stall angle of attack for the single and leading airfoils. Then negative $C_d(t)$ indicates that the trailing airfoil is generating thrust at a post-stall angle of attack, which can be a major advantage.

Finally, as seen in Fig. 13a there is almost no wake roll-up for airfoil A, while airfoil B has roll-up similar to the single airfoil with traces of a secondary roll-up.

3.7 Effect of Only the Leading Airfoil Pitching on Configuration of Airfoils

Results presented here are for a case study of tandem airfoils, where only the leading airfoil is pitching:

$$\alpha_A = 3^{\circ} + 10\sin\omega t; U_{\infty} = 15m/s; \omega_A = 1^c/s, 3^c/s$$

The trailing airfoil is stationary at:

$$\alpha_B = 5^{\circ}; \quad U_{\infty} = 15m/s; \quad \frac{d}{c} = 1.5$$

As seen in Fig. 14a the lift-hysteresis is nominal for the leading airfoil. On the other hand, it is interesting to note that although the trailing airfoil is not pitching, its C_l undergoes a sinusoidal pattern. The C_d in Fig. 14c shows considerable hysteresis for the leading airfoil while that for the trailing airfoil hovers around zero accompanied by negative spikes. As seen in Fig. 15a and 15b the leading airfoil has nearly zero wake roll-up while the trailing airfoil shows limited wake roll-up for $\omega_A = 1rad/s$ but considerable wake roll-up for $\omega_A = 3rad/s$ along with marked secondary roll-up. This can be explained using Figs 15c and 15d, which shows large hysteresis in Γ_w for airfoil A. For airfoil B, Γ_w is not significant and hovers around zero for $\omega_A = 1rad/s$ but for $\omega_A = 3rad/s$ it is signifi-cant and marked by both positive and negative peaks.

4. CONCLUSION

A numerical study of the flow-field around tandem airfoils exhibiting unsteady motion is undertaken using an unsteady discrete vortex method. Various cases of un-steady motion are studied to gain insights

into the effect of the trailing edge vortices on the performance of the airfoils. Interaction of free wake vortices with the air-foils as well as with each other is studied. While a free wake vortex dissipates as it encounters an airfoil, numerical singularity arises when two such vortices come very close to each other.

It is found that the counter-clockwise trailing edge vortex shed from the leading airfoil in the immediate time-instant is very strong and its effect on both the air-foils dominates the flow field, namely causing a strong downwash on the leading airfoil and a strong upwash on the trailing airfoil. As it moves downstream, its effect on the airfoils wanes. However, as it crosses the leading edge of the trailing airfoil, due to its position, the counter-clockwise vortex now causes a strong downwash on the trailing airfoil. As a result, the circulation of the trailing airfoil changes abruptly resulting in abrupt changes in its C_l and C_d .

Strong wake roll-up is seen for the trailing airfoil due to the additional circulation of the trailing edge vortex shed by the leading airfoil as well as that shed by the trailing airfoil itself. For the leading airfoil on the other hand, there is no significant wake roll-up.

The effect of relative velocity, rates of pitching and phase lag on the strength of the trailing edge vortex and its movement is found to be significant. Hence, the method developed here is simple and effective to study the flow-field around interacting airfoils.

REFERENCES

Bacic, M. (2008). On prediction of aircraft trajectory at high-angles of attack: Preliminary Results for a Pitching Airfoil. In *Proc AIAA Model Simul. Technol. Conf.*

Capece VR, Fleeter S. Wake Induced Unsteady Aerodynamic Interactions in a Multi-Stage Compressor, AIAA 1986-1455.

Chorin, A. J. and P. S. Bernard (1973). Discretization of a vortex sheet, with an example of roll-up. *J. of Computational Physics* 13(3), 423-429.

Fage, A. and F. C. Johansen (1927). On the flow of air behind an inclined flat plate of infinite span. *Proc. Roy. Soc* A 116, 170.

Fritz, T. and L. N. Long (2004). Object-Oriented Unsteady Vortex Lattice Method for Flapping Flight. *Journal of Aircraft* 41(6), 1275-1290.

Fulayter, R. D., P. B. Lawless and S. Fleeter (2002). Rotor Generated Vane Row Off-Design Unsteady Aerodynamics Including Dynamic Stall: Part II: 3-D Rotor Wake Forcing Function & Stator Unsteady Aerodynamic Response. *AIAA- 3543*

Greenwell, D. G. (2004). A review of unsteady Aerodynamic Modeling for Flight Dynamics of Maneuverable Aircraft. *AIAA. - 5276*

Hall, K. C. and W. S. Clark (1993). Linearized Euler Predictions of Unsteady Aerodynamic Loads in Cascades. *AIAA Journal* 31(3), 540-550.

Husain, Z., M. J. Abdullah and T. C. Yap (2005). Two-dimensional analysis of tandem/staggered airfoils using computational fluid dynamics. *International Journal of Mechanical Engineering Education* 33(3), 195.

Jose, A. I. and J. D. Baeder (2009). Steady and Unsteady Aerodynamic Modeling of Trailing Edge Flaps with Overhang and Gap using CFD and Lower Order Models. *AIAA. - 1071*

Katz, J. and B. Maskew (1988). Unsteady low-speed aerodynamic model for complete aircraft configurations. AIAA Paper 1986-2180; J. Aircraft, 25(4), 302-310.

Katz, J, and A. Plotkin (1988). *Low-speed Aerodynamics*. Cambridge University Press, 2001. Nakagawa T. On Unsteady Airfoil-Vortex Interaction, ACTA MECHANICA 75, 1-13.

Katz, J. and D. Weihs (1978). Behaviour of vortex wakes from oscillating airfoils. *J. Aircraft* 15(12), 861-863.

McCroskey, W. J., K. W. McAlister, L. W. Carr, S. L. Pucci SL, O. Lambert and R. F. Indergrand (1981). Dynamic stall on advanced airfoil sections. *J. Amer. Helicopter Soc.* 26(3), 40-50.

Radmanesh, M., O. Nematollahi1, M. Nili-Ahmadabadi1 and M. Hassanalian (2014). A Novel Strategy for Designing and Manufacturing a Fixed Wing MAV for the Purpose of Increasing Maneuverability and Stability in Longitudinal Axis. *JAFM* 7(3), 435-446.

Platzer, M. F., K. S. Neace and C. K. Pang (1993). Aerodynamic analysis of flapping wing propulsion. *AIAA*. - 0484

Shokrgozar, A., A. B. Rahimi and H. Mozayyeni (2016). Investigation of Three-Dimensional Axisymmetric Unsteady Stagnation-Point Flow and Heat Transfer Impinging on an Accelerated Flat Plate. *Journal of Applied Fluid Mechanics* 9(1), 451-461. 2016.

Wagner, H. Uber die Entstehung des Dynamischen Autriebes von Tragflugeln, Z.F.A.M.M., Vol. 5, No. 1, pp 17-35, 1925.

Wu, J. C., C. M. Wang and I. H. Tuncer (1986). Unsteady Aerodynamics of Rapidly Pitched Airfoils. *AIAA. - 1105*